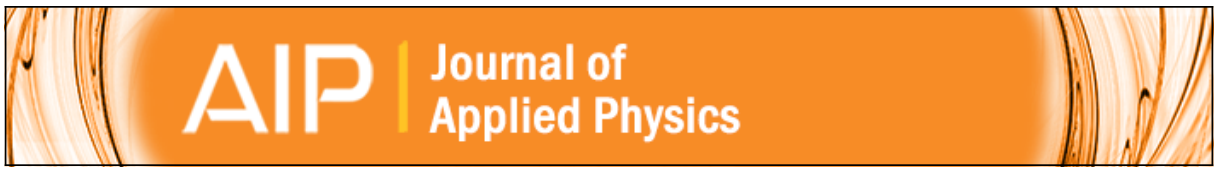

Wave attenuation and dissipation mechanisms in viscoelastic phononic crystals

Joo Hwan Oh, Yoon Jae Kim, and Yoon Young Kim

Citation: Journal of Applied Physics **113**, 106101 (2013); doi: 10.1063/1.4795285
View online: http://dx.doi.org/10.1063/1.4795285
View Table of Contents: http://scitation.aip.org/content/aip/journal/jap/113/10?ver=pdfcov
Published by the AIP Publishing

Wave attenuation and dissipation mechanisms in viscoelastic phononic crystals

Joo Hwan Oh,[1] Yoon Jae Kim,[2] and Yoon Young Kim[1,a)]
[1]*WCU Multiscale Design Division, School of Mechanical and Aerospace Engineering, Seoul National University, 599 Gwanak-ro, Gwanak-gu, Seoul 151-744, South Korea*
[2]*The 7th R&D Institute-2, Agency for Defense Development, Yuseong PO Box 35, Daejeon 305-600, South Korea*

(Received 20 December 2012; accepted 28 February 2013; published online 13 March 2013)

This work investigates wave attenuation and dissipation mechanisms in viscoelastic phononic crystals (VPCs) having different inclusion types in a long-wavelength regime. After investigating the intrinsic damping properties of VPCs for different inclusion sizes and materials, we carried out wave simulations revealing the energy dissipation by a finite VPC structure inserted inside an elastic medium. The simulations, supported by physical reasoning, showed that air- and metal-embedded VPCs can indeed dissipate more wave energy than pure viscoelastic media in low and high frequency ranges, respectively. © *2013 American Institute of Physics*. [http://dx.doi.org/10.1063/1.4795285]

In this work, we aim to investigate how and why the overall damping properties of viscoelastic phononic crystals (VPCs) are affected by the types (material and size) of VPCs, especially in the frequency range where wavelengths are much larger than the VPC unit cell size (see, e.g., Ref. 1 for theories on viscoelasticity). Several researchers previously studied the band structure of VPCs,[2] but investigations on wave attenuation of VPCs are relatively limited. The effect of the mode conversion[3] and the local resonance[4] to the attenuation of VPCs has been investigated, but the frequency ranges considered in these works were relatively higher or narrower than the range focused on this work. Targeting at a broad low-frequency range, attenuation in VPCs made of a viscoelastic matrix and hollow glass spheres has been studied.[5] However, the detailed wave phenomena taking place inside VPCs were not given so that attenuation mechanisms in VPCs need to be further investigated.

In this study, two types of VPCs made of a viscoelastic rubber matrix and circular inclusions with varying sizes are considered. Type 1 will consider air inclusions and Type 2, tungsten inclusions. Air may be regarded as a representative material softer than the matrix, while tungsten, a harder material. For all types, inclusions are periodically arranged to form a square-lattice crystal whose unit cell size is $8 \times 8\,\mathrm{mm}^2$. Here, wave attenuation in the long-wavelength frequency range (from 30 Hz to 3000 Hz) is mainly focused.

When the host viscoelastic material is modeled by a linear viscoelastic theory,[1] its damping effect can be expressed in terms of a complex-valued stiffness matrix C^*, which can be written as

$$C^* = C(1 + i\tan\delta)\,(i = \sqrt{-1}), \tag{1}$$

where $\tan\delta$ is the loss-tangent of a viscoelastic material. In case of rubber, it can be approximated as $\tan\delta = 0.1512 + 2\pi \times 1e-4 \times \omega$ (Ref. 6) where ω denotes angular frequency. Other material properties needed for simulations are listed here: c_l (longitudinal wave velocity) $= 1469\,\mathrm{m/s}$, c_t (transverse wave velocity) $= 360\,\mathrm{m/s}$, and ρ (density) $= 1039\,\mathrm{kg/m^3}$ for rubber, and $c_l = 5027\,\mathrm{m/s}$, $c_t = 2822\,\mathrm{m/s}$, and $\rho = 17\,800\,\mathrm{kg/m^3}$ for tungsten. Air inclusions are modeled with $c_l = 330\,\mathrm{m/s}$, $c_t = 0\,\mathrm{m/s}$, and $\rho = 1\,\mathrm{kg/m^3}$.

To calculate the wave attenuation and the effective loss-tangent of a VPC, the following procedure is used. First, the complex band structure for a VPC is determined by the extended plane-wave expansion method.[7] Here, only in-plane longitudinal bulk waves are considered. Then, the complex wavevectors $k = \alpha + i\beta$ (α, β : real) are determined from the calculated band structure at desired frequencies. Finally, the attenuation and effective loss-tangent can be calculated from the complex wavevectors as[8]

$$\begin{aligned}\text{Attenuation} = \beta,\ \text{Loss} - \text{tangent} \\ = imag(\bar{\rho}\omega^2/k^2)/real(\bar{\rho}\omega^2/k^2),\end{aligned} \tag{2}$$

where $\bar{\rho}$ is the effective density of a VPC. At low frequencies, $\bar{\rho}$ for PCs having circular inclusions can be calculated as $\bar{\rho} = \rho_{matrix}V_{matrix} + \rho_{inclusion}V_{inclusion}$,[9] where V_{matrix} and $V_{inclusion}$ denote the volume fractions of the matrix and inclusion, respectively. Note that the attenuation is related to decrease in wave amplitude along the propagating direction. The loss-tangent is related to the ratio of the time-averaged dissipated energy density with respect to the time-averaged total energy density.[8] The values of the attenuation and effective loss-tangent for the two VPC cases are shown in Fig. 1. The values in Fig. 1 are obtained for 30 Hz, but they are almost unaltered at all other frequencies considered in this work.

In case of air inclusion (Type 1), the attenuation monotonically increases as the size of the inclusion increases while the effective loss-tangent almost remains unaffected regardless of the size variation of the inclusion. To explain these phenomena, the mode shape of the longitudinal wave and its power distribution in the x direction are plotted in Fig. 2(a). It shows that the wave power mainly flows through the matrix

a)Author to whom correspondence should be addressed. Electronic mail: yykim@snu.ac.kr. Tel.: +82-2-880-7154. Fax:+82-2-872-1513.

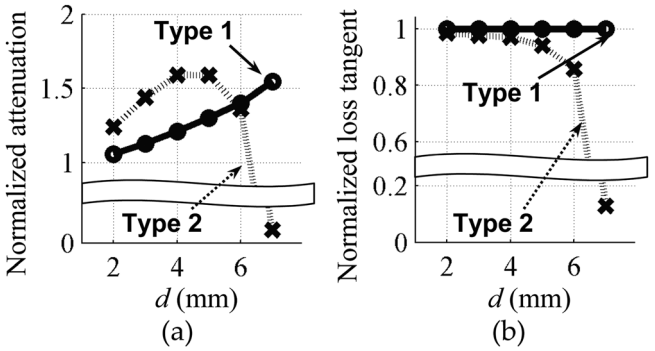

FIG. 1. The values of (a) the normalized attenuation and (b) normalized effective loss-tangent for varying inclusion sizes in VPCs of Type 1 and Type 2. Here, d is the inclusion's diameter.

irrespective of the inclusion size, although inclusions are also deformed. So, the amount of the time-averaged dissipated energy density will remain the same. Because the effective loss-tangent will not change for the same ratio of the time-averaged dissipated energy to the time-averaged total wave energy, its value will be almost the same irrespective of the inclusion size as apparent in Fig. 1(b). On the other hand, Fig. 3(a) shows that the wave speed in the VPC of Type 1 monotonically decreases as the inclusion size increases. As explained in previous slow light investigations,[10] slow waves result in higher amplitudes, yielding larger damping force per length. The comparison of the attenuation in Fig. 1(a) and the wave speed in Fig. 3(a) suggests that the attenuation is almost inversely proportional to the wave speed. Therefore, the change in the wave speed is found to be responsible for the change in the attenuation for Type 1.

The situation for Type 2 is quite different from that of Type 1. The attenuation increases until the size of the tungsten inclusion reaches $d = 4$ mm, and it decreases afterwards.

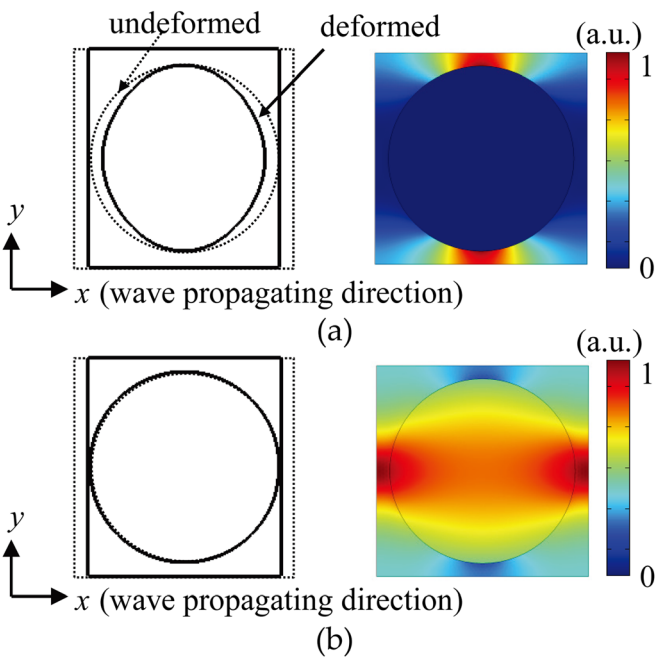

FIG. 2. The mode shape (left) and the x-directional wave power (right) for the longitudinal waves propagating at 30 Hz in the 8×8 mm^2 VPCs with $d = 7$ mm. (a) Type 1 and (b) Type 2.

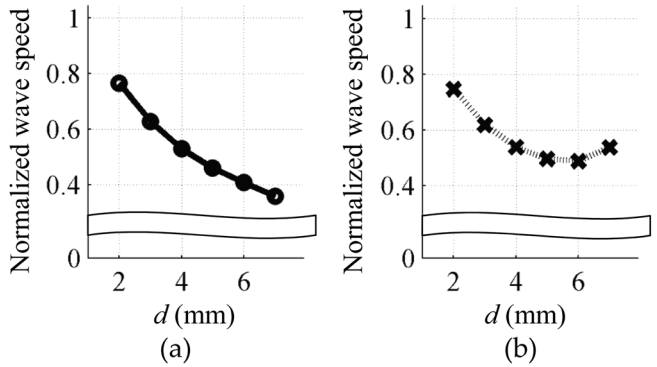

FIG. 3. The longitudinal phase velocity for varying inclusion size at 30 Hz for (a) VPC of Type 1 and (b) Type 2. The material loss in rubber is ignored in the calculation of the phase velocity. (Normalized as in Fig. 1).

On the other hand, the effective loss-tangent decreases monotonically as d increases. Because tungsten is a harder material than the matrix, considerably a large amount of wave energy passes through the tungsten inclusions, as shown in Fig. 2(b). Note that wave energy inside the inclusions is not dissipated. Therefore, the amount of the time-averaged dissipated energy density and the effective loss-tangent become reduced as the inclusion size increases, as demonstrated in Fig. 1(b). On the other hand, Fig. 3(b) indicates that the speed decreases as d increases, but it increases as d becomes larger than a certain value d^* (in the present case, $d^* = 6$ mm). When d is smaller than d^*, the inclusion acts as a rigid mass while the rubber matrix acts as a spring, meaning that the stiffness effect of the inclusion can be ignored.[9] Therefore, increasing the inclusion size is equivalent to adding more mass in the system, lowering the wave speed. When d becomes larger than d^*, the stiffness of the inclusion is brought into play,[9] and also wave propagation through the tungsten inclusion becomes more significant. Consequently, the wave speed becomes larger. Therefore, both the wave speed and effective loss-tangent are responsible for the change in the attenuation for Type 2.

Let us now investigate the effectiveness of finite VPC structures when they are inserted in an elastic medium. For the investigation, a one-dimensional wave simulation model presented in Fig. 4 is adopted. For time-harmonic simulations carried out with COMSOL,[11] either Type 1 or Type 2 VPC structure composed of 10 unit cells is inserted in the middle of an elastic Lucite medium ($c_l = 2672$ m/s, $c_s = 1091$ m/s, and $\rho = 1200$ kg/m^3), and the following dissipation measure is calculated:

$$\xi = 1 - (P_T + P_R)/P_I, \tag{3}$$

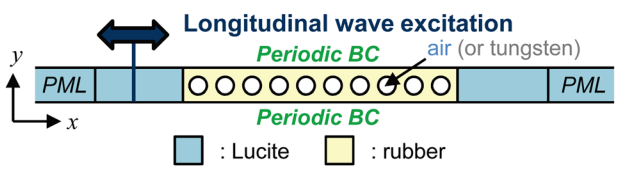

FIG. 4. Finite element time-harmonic wave simulation model of the VPC inserted inside an elastic body.

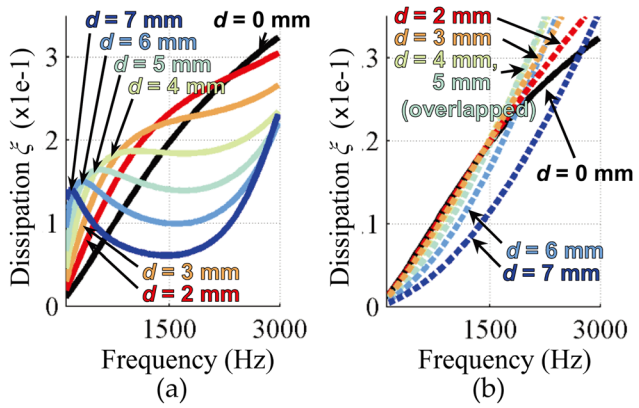

FIG. 5. Dissipation ξ calculated with the simulation model in Fig. 4. (a) Type 1 and (b) Type 2.

where P_I, P_T, and P_R denote the incident, transmitted, and reflected wave powers, respectively. The two point method[12] was used to calculate P_R and P_I.

The calculated values of the dissipation measure ξ in Fig. 5 show significant effects of the inclusion type; ξ tends to increase at low frequencies for Type 1 while it does at high frequencies for Type 2. To explain these phenomena, we note that ξ is mainly affected by the following three factors: (1) the intrinsic attenuation of the VPC (as studied above), (2) the amount of the energy transmitted from the left Lucite medium to the VPC structure, and (3) the amount of the energy trapped in the VPC. The trapped energy is due to multiple-reflected waves from both boundaries of the VPC structure.

In case of Type 1, both the effective density and wave speed decrease as the inclusion size increases. As a result, mismatch between the high impedance of the Lucite medium and the low impedance of the VPC will increase. Since waves can be transmitted sufficiently well from a high-impedance medium into a low-impedance medium at low frequencies (corresponding to waves of much longer wavelength than the size of the VPC structure), the amount of the transmitted energy from the left Lucite to the VPC structure is quite significant. Therefore, ξ is dominantly controlled by Factors 1 and 3, not by Factor 2. If the impedance difference becomes larger, more energy can be trapped in the VPC structure, resulting in larger ξ values. In this situation, the attenuation also increases as in Fig. 1(a). Thereby, one can now explain why ξ increases at low frequencies for the Type 1 VPC as d increases. At high frequencies, however, wave transmission from the left Lucite to the VPC is affected significantly by the impedance mismatch, making ξ most affected by Factor 2. Since little energy is transmitted into the VPC, other factors become less influential. Consequently, ξ decreases at high frequencies for the Type 1 VPC as d increases.

In case of Type 2, the introduction of inclusions in the rubber matrix may decrease the wave speed in the VPC but considerably increases the effective density of the VPC. Thus, the difference between the impedance of the VPC and that of the Lucite medium becomes reduced as d increases. While the severity of impedance mismatch does not influence much the transmitted energy into the VPC structure at low frequencies, the reduction in the impedance mismatch will affect Factor 3. This reasoning explains why ξ decreases as d increases at low frequencies. In contrast, the reduced impedance mismatch influences Factor 2 mostly at high frequencies, and thus it increases ξ. However, the attenuation of Type 2 VPC significantly drops when d reaches 5 mm (see Fig. 1(a)). Therefore, the drop is primarily responsible for the decreasing ξ values for $d > 5$ mm.

This study investigated how the type (material) of inclusions in a VPC affects its damping properties. While air-embed VPCs exhibit similar wave behavior regardless of excitation frequencies, metal-embed VPCs do not. The specific amount of dissipated wave energy will be affected by the selected VPC materials and the operating frequency, but the findings from this study will remain valid for any VPC.

This work was supported by the National Research Foundation of Korea (NRF) (Grant No. 20120005693) funded by the Korean Ministry of Education, Science and Technology (MEST) contracted through IAMD at Seoul National University and the WCU program (No. R31-2008-000-10083-0) through NRF funded by MEST.

[1]R. M. Christensen, *Theory of Viscoelasticity* (Academic, New York, 1971).
[2]M. I. Hussein, Phys. Rev. B **80**, 212301 (2009); Y. Liu, D. Yu, H. Zhao, J. Wen, and X. Wen, J. Phys. D: Appl. Phys. **41**, 065503 (2008); B. Merheb, P. A. Deymier, M. Jain, M. Aloshyna-Lesuffleur, S. Mohanty, A. Berker, and R. W. Greger, J. Appl. Phys. **104**, 064913 (2008); R. Moiseyenko and V. Laude, Phys. Rev. B **83**, 064301 (2011).
[3]H. Zhao, Y. Liu, D. Yu, G. Wang, J. Wen, and X. Wen, J. Sound Vib. **303**, 185 (2007); H. Zhao, J. Wen, D. Yu, and X. Wen, J. Appl. Phys. **107**, 023519 (2010).
[4]J. Mei, G. Ma, M. Yang, Z. Yang, W. Wen, and P. Sheng, Nat. Commun. **3**, 756 (2012).
[5]G. C. Gaunaurd and H. Uberall, J. Acoust. Soc. Am. **71**, 282 (1982); G. C. Gaunaurd and J. Barlow, *ibid.* **75**, 23 (1984); A. M. Baird, F. H. Kerr, and D. J. Townend, *ibid.* **105**, 1527 (1999); H. Zhao, Y. Liu, J. Wen, D. Yu and X. Wen, J. Appl. Phys. **101**, 123518 (2007).
[6]T. R. Lin, N. H. Farag, and J. Pan, Appl. Acoust. **66**, 829 (2005).
[7]V. Laude, Y. Achaoui, S. Benchabane, and A. Khelif, Phys. Rev. B **80**, 092301 (2009).
[8]B. A. Auld, *Acoustic Fields and Waves in Solids* (Krieger, Florida, 1990).
[9]B. Hassani and E. Hinton, *Homogenization and Structural Topology Optimization* (Springer, London, 1999).
[10]T. F. Krauss, Nat. Photonics **2**, 448 (2008); M. Soljacic and J. D. Joannopoulos, Nat. Mater. **3**, 211 (2004).
[11]COMSOL MULTIPHYSICS, *COMSOL Multiphysics Modeling Guide: Version 3.5* (COMSOL AB, Stockholm, 2008).
[12]B. Lundberg and A. Henchoz, Exp. Mech. **17**, 213 (1977).